Thermomechanical controlled processing to achieve very fine grains in the ISO 5832-9 Austenitic Stainless Steel Biomaterial

Mariana Beatriz dos Reis Silva[1], Jose Maria Cabrera[2], Oscar Balancin[1] and Alberto Moreira Jorge Jr[1,3 *]

[1] Department of Materials Engineering, UFSCar, Via Washington Luis, Km 235, 13565-905 São Carlos, SP, Brazil

[2] Department of Materials Science and Metallurgical Engineering, Technical University of Catalunya – Barcelona Tech, Av. Diagonal 647, 08028 Barcelona, Spain

[3] Univ. Grenoble Alpes, SIMAP and LEPMI, CNRS, SIMAP, 38000 Grenoble, France

[*]Corresponding author: moreira@dema.ufscar.br

* Phone: +55 16 33518531 - Fax :+55 16 33615404

Abstract

Simulations of thermomechanical processing of a high niobium- and nitrogen-bearing austenitic stainless steel for orthopedic implants (ISO 5832-9) were conducted using hot torsion test with multiple deformations under continuous cooling conditions. Samples were reheated to 1250^{o}C and subjected to deformation schedules with pass strain of 0.3, strain rate of 1 s^{-1} and interpass times of 5, 20 and 50 seconds. Optical microscopy, TEM, EDS and EBSD were used to characterize the samples. Characterization of precipitates indicated that only TiNbN was undissolved after soaking, while Z-phase and NbN precipitated during on cooling deformation schedules. The evolution of grain and precipitate sizes with deformation conditions were studied and related to both grain refinement, and mechanical behavior observed. The critical grain size limited by precipitates was calculated using the values obtained for size and volume fraction of precipitates. Differences observed between calculated and measured values were discussed.

***Keywords*:** Thermomechanical controlled processing, Niobium, Strain-induced precipitation, Recrystallization, Grain Refinement, Stainless steel.

Thermomechanical controlled processing to achieve very fine grains in the ISO 5832-9 Austenitic Stainless Steel Biomaterial

Abstract

Simulations of thermomechanical processing of a high niobium- and nitrogen-bearing austenitic stainless steel for orthopedic implants (ISO 5832-9) were conducted using hot torsion test with multiple deformations under continuous cooling conditions. Samples were reheated to 1250^{o}C and subjected to deformation schedules with pass strain of 0.3, strain rate of 1 s^{-1} and interpass times of 5, 20 and 50 seconds. Optical microscopy, TEM, EDS and EBSD were used to characterize the samples. Characterization of precipitates indicated that only TiNbN was undissolved after soaking, while Z-phase and NbN precipitated during on cooling deformation schedules. The evolution of grain and precipitate sizes with deformation conditions were studied and related to both grain refinement, and mechanical behavior observed. The critical grain size limited by precipitates was calculated using the values obtained for size and volume fraction of precipitates. Differences observed between calculated and measured values were discussed.

***Keywords*:** Thermomechanical controlled processing, Niobium, Strain-induced precipitation, Recrystallization, Grain Refinement, Stainless steel.

1 - INTRODUCTION

The needs for high strength, corrosion resistance, workability and weldability make austenitic stainless steels an attractive alternative for several industry segments, extending their applications in everyday life such as household items to those found in aggressive media like in the extraction and processing of gas and oil, industries such as textile, chemical, shipbuilding, automotive, aerospace, buildings and orthopedic implants [1-3]. Specifically, in orthopedic implants, high nitrogen austenitic stainless steels have been applied because this element has a crucial role in stabilizing non-magnetic austenite, increasing strength and preventing pitting corrosion.

The stainless steel for orthopedic implants according to ISO 5832-9 is an stainless steel with high nitrogen (0.35%) and niobium (0.28%) contents that has been used as an alternative to ASTM F138 (a widely used steel for implants, with high nitrogen but without niobium) because it exhibits low strength in the annealed condition and susceptibility to localized corrosion [4]. However, there are few works in the literature about the formability of such steel, and a better understanding of hardening and softening mechanisms involved during its thermomechanical processing would help in optimizing its performance in service and also in improving the processing of similar steels, mainly those with a high content of nitrogen and niobium.

In previous publications, the plastic behavior of this steel was detailed studied under isothermal conditions by single and double hot high deformation tests. The shape of flow curves, the constitutive equations for such curves, processing maps and the evolution of the microstructure were determined and analyzed in the temperature range between 900 and 1200°C and strain rates ranging from 0.01 to 10 s-1 [5,6]. The results showed a strong competition between recovery and recrystallization, with a significant

amount of recovery, regions with high plastic instability and precipitation of a second phase identified as Z-phase. In addition, more recently [7] we have partially characterized this material using interpass times of 5 and 20 s, leaving uncertainties about its behavior for longer interpass times, which are closer to the industrial conditions.

The Z-phase is a complex nitride that forms in steels stabilized with Nb containing high nitrogen, and has been characterized by X-ray diffraction as tetragonal having Cr, Nb, and N and lattice parameters a = 3.037 Å and c = 7.391 Å [8, 10]. This phase is stable at high temperatures. Its solubilization temperature depends upon the chemical composition and may change from one grade to another. Therefore, even though in the same temperatures, different grades can form either small or coalesced precipitates. When the particles are small, they tend to decrease the mobility of grain boundaries formed upon straining by dynamic recrystallization and during the interpass time by static and metadynamic recrystallization. In turn, when precipitates coalesce, a degradation of fatigue properties and corrosion resistance of the material is noticed [11-16]. The formation of Z-phase is unclear at present and not well established whether it is formed from prior nitride precipitates as proposed by some authors [13, 17-19] or directly nucleated as suggested by others [8, 20, 21]. Indeed, as far as the present authors know, the solubility product of this phase has not been yet reported.

In the thermomechanical processing of steels, the re-precipitation of particles dissolved during soaking is extremely important, because size and distribution of new precipitates are responsible for the effectiveness of controlling the grain size. Furthermore, the presence of solute can decrease the mobility of grain and subgrain boundaries and, therefore, can alter the recrystallization kinetics and in consequence,

modify the final grain size. In this sense, it is very well known the role played by Nb in delaying dynamic and static recrystallization [22].

During the thermomechanical processing of metals, there is a competition between the driving force for recrystallization that arises from the stored energy due to the deformation and pinning force exerted by precipitates and solid solution atoms. Indeed, this competition dictates the recrystallization-precipitation interaction. This interaction controls the final microstructure and, therefore, the ultimate mechanical properties. Thus, for an appropriate design of a thermomechanical process, it is mandatory a considerable understanding of such interaction [7, 23].

The strict control of thermomechanical processing involves many variables such as reheating temperature, cooling rate, strain, strain rate and interpass times. Such a large number of parameters hinder the study of operative mechanisms. Bearing in mind these features, in this work, the interaction between recrystallization and precipitation of a stainless steel for orthopedic implants with high N and Nb (ISO 5832-9) was investigated paying special attention to the effect of the interpass time. It was measured and analyzed the evolution of grain and precipitate sizes and their correlation with mechanical behaviors during deformation schedules.

2 - EXPERIMENTAL PROCEDURE

The chemical composition of the high-nitrogen niobium austenitic stainless steel for orthopedic implants, ISO 5832-9, analyzed in this work is listed in the Supplementary Table S1. The steel was supplied by Villares Metals (Brazil), hereafter called VI 58329 (the code received from Villares Metals for the ISO 5832-9 standard). It has been received as bars with 20 mm in diameter after hot rolling and annealing at

1030°C for 60 min and water cooling. A number of physical simulation experiments were carried out in a computer-controlled hot torsion machine (please, see details in the Supplementary Methodology) on cylindrical specimens machined out from the bars, with an effective radius of 5 mm and 10 mm in length in the reduced central gage section.

The samples were heated to1250°C at a rate of 5.5°C/s and held at this temperature for 300 s. Interpass times of 5, 20 and 50 s were applied between successive deformations of 0.3 and strain rate of $1s^{-1}$, under continuous cooling conditions. The experiments were interrupted after the 2^{nd}, 6^{th} and 13^{th} deformations passes. In order to maintain the same temperature for each pass regardless the interpass time, different cooling rates were imposed: 24^{o}C/min for the interpass time of 50 s, 60^{o}C/min for the interpass time of 20 s and 240^{o}C/min for the interpass time of 5s. The microstructures were observed below the deformed surface, in a longitudinal plane. Optical microscopy, electron backscatter diffraction (EBSD) and transmission electron microscopy (TEM) were used to characterize the microstructure after every test. Please, refer to Supplementary Methodology for more details of the Experimental Procedure.

The precipitated particle densities were calculated by dividing the number of precipitates found (over than 200) by the total area analyzed. Calculation of volume fractions (V_f) were performed according to the equation proposed by Maniar [24]:

$$V_f = \frac{\pi}{3} \times \frac{N_r}{A_r} \times \frac{d^3}{d_{\max}}$$

where N_r is the number of particles counted, A_r the analyzed area, d is the average particle diameter and d_{max} is the diameter of the largest particle in the analyzed area.

3 - RESULTS

3.1 Flow curves

Flow stress curves for VI 58329 steel tested with interpass times of 5, 20 and 50 s after a soaking temperature of 1250°C are displayed in Supplementary Fig. S1. Another conventional way to identify the microstructural evolution during simulation of the thermomechanical processing is the graph of the mean flow stress (MFS), for each pass, as a function of the inverse of the absolute temperature, as shown in Fig. 1. MFS was calculated using the equation proposed by Boratto et al [25].

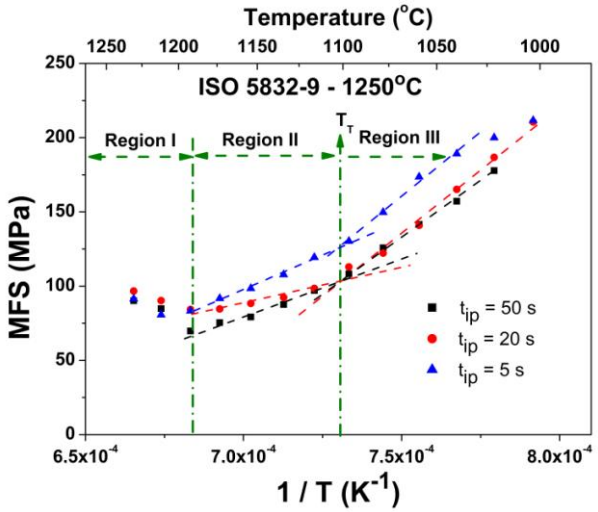

Fig. 1. Dependence of the mean flow stress (MFS) with the inverse of absolute temperature (1/T), where t_{ip} is the interpass time

Both Figures (1 and S1) present the same general trend (please, see Supplementary Fig. S1 for comparison). In other words, the flow stresses under continuous cooling condition increases with the pass number except in the first three passes. The stress level at the first pass is greater than at the second pass, and this is larger than at the third pass. Only after the third pass, the stress level increases due to the temperature decreasing. At the very lower temperatures, the stress level increases

more markedly.

The diagram MFS *vs*. 1/T presented in Fig. 1 emphasizes the three distinct regions, namely: I) at the highest temperatures, the material was hardened in the first pass and then was softened in the two subsequent passes; II) after the third pass, the stress level increases due to the temperature decreasing; III) at lower temperatures, along with the decrease in temperature, there is evidence that another strengthening mechanism is acting due to a change in the slope of the curves. This specific behavior will be discussed later, after presentation regarding precipitation results. However, it can be expected that there is a transition temperature ($\mathbf{T_T}$ = around 1100^{o}C) similar as no recrystallization temperature (T_{nr}) found in microalloyed steels. Instead T_{nr}, T_T is being used because, in the case of the steel VI 58329, the precipitation is not as efficient to completely cease the recrystallization, as it is the case for microalloyed steels. By definition, T_{nr} defines the transition from full crystallization to no recrystallization.

3.2 Microstructural evolution

3.2.1 Optical microscopy

Supplementary Fig. S2 displays optical micrographs of the VI 58329 in the conditions of as-received and after reheating. The microstructure in as-received condition (Supplementary Fig. S2.a) was quite homogeneous with average grain size of 14.4 μm and large precipitates inside the grains and at grain boundaries. After reheating, Supplementary Fig. S2.b, the microstructure displayed a large number of coarse particles of different sizes. These particles were not dissolved during the soaking time. Furthermore, it was observed a heterogeneous grain size distribution, due to the appearance of an abnormal growth. Keeping in mind this heterogeneity, the average

grain diameter was 61.8 µm. Annealing twins were also apparent. This latter condition was considered as the starting microstructure before the multiple hit torsion tests since all samples were reheated at the same temperature for the same holding time.

Optical micrographs displayed in the Supplementary Fig. S3 present the microstructural evolution as a function of the pass number (2, 6 or 13 passes) and interpass times (5, 20 or 50 s). These samples were quenched just after interpass times. All microstructures in Fig. S3 are displayed under the same magnification for better visualization of the evolution of grain size. Analysis of samples with very fine grain sizes was also performed at higher magnifications as shown later in the EBSD study.

In all conditions, either for 2 or 6 passes, it was observed a fully recrystallized and homogeneous microstructure. However, even with optical microscopy, one can observe that the samples with interpass time of 50 s presented larger precipitates in higher quantity than those observed after 20 and 5 s. No significant differences were observed between the grain sizes after 2 passes with interpass times of 50 and 20 s, neither between 2 and 6 passes with an interpass time of 50 s. In these three cases, the average grain sizes were close to 33 µm. However, the grain refinement increases with the number of passes and the decreasing of interpass time. The 13th pass was conducted below the transition temperature, and accordingly, an intense grain refinement was observed. It is worth noting that under the latter conditions, the microstructures showed some slightly elongated grains (lighter regions in the pictures) and smaller recrystallized grains. This may be related to the fact that full recrystallization was not achieved, as will be discussed later. Furthermore, one can observe that, at the end of the thermomechanical processing, the grain size was reduced by half with interpass time reduced by 10 times: measurements gave an average grain size of about 11.1 µm with

an interpass time of 50 s, 9.5 µm for 20s and 5.1 µm for 5 s. Figure 2 summarizes the evolution of grain diameters as a function of the interpass time.

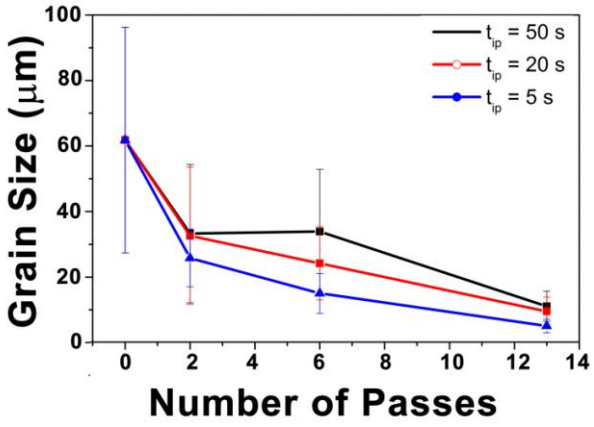

Fig. 2. Grain size evolutions as a function of the number of passes

3.2.2 EBSD analyses

To investigate whether dynamic recrystallization occurred or not during the deformation schedules, complementary experiments under similar conditions were conducted. However, for this, two sets of samples were produced: one quenched immediately after the deformation and other quenched after the interpass time. Fig. 3 displays microstructures observed in samples quenched immediately after the 2nd and 6th passes, with an interpass time of 20 s. The first figure of each condition, Fig. 3a (2nd pass) and Fig. 3c (6th pass), represent maps of the image quality (IQ), which are a direct measure of the intensity of Kikuchi' bands, related to the sample preparation and its surface quality. If one considers that the sample surface was well-prepared and that for the indexation only the phase related to the matrix was inserted (please, refer to Supplementary Methodology), in the gray scale generated in these maps, particles appear as black spots due to the low quality of the patterns for the particulate zones. Low-quality patterns will also occur in grain boundaries, which appear as dark lines. It can be seen in these maps the presence of elongated grains surrounded by small grains in a

growing process so-called the necklace mechanism that is a typical evidence of dynamic recrystallization appearance. In consequence dynamic recrystallization took place in the first passes and is the major mechanism responsible for grain refinement.

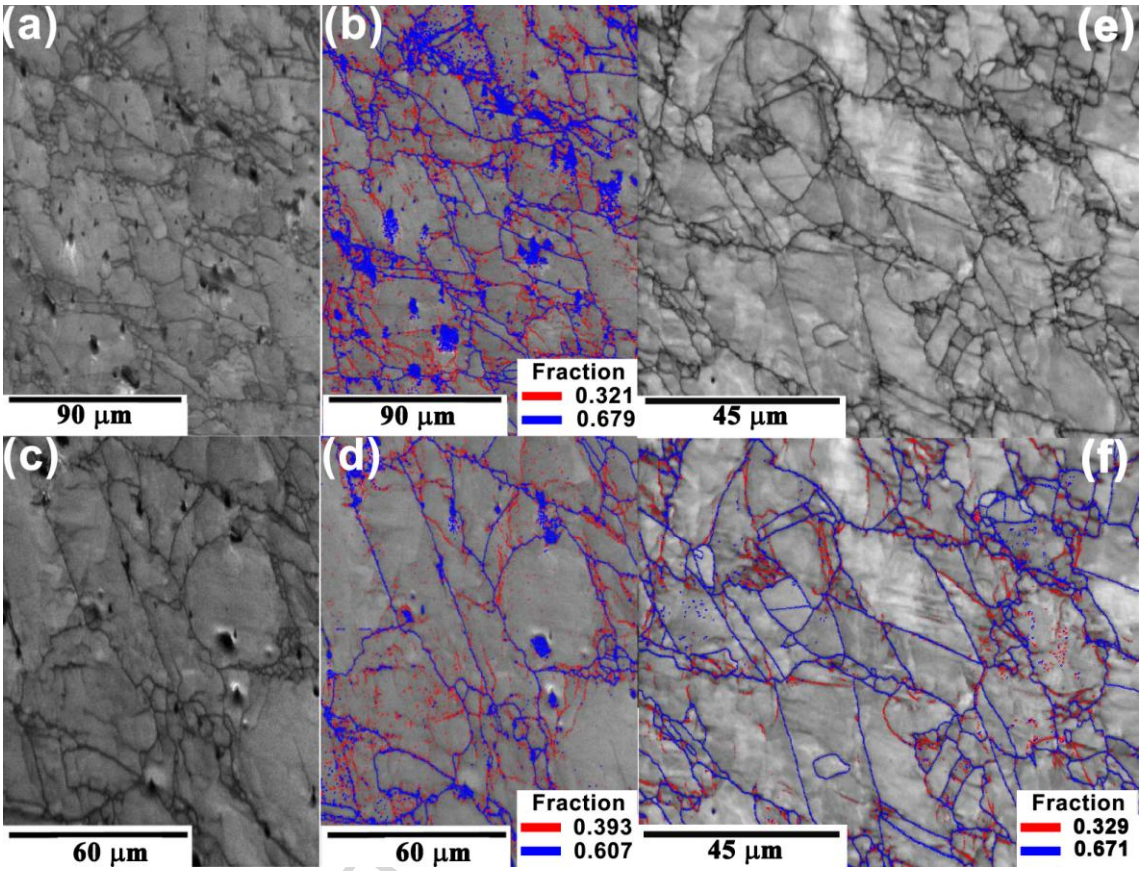

Fig. 3. Maps obtained by EBSD from samples water-cooled immediately after deformations with interpass time of 20 s: (a) and (b) sample with 2 passes; (c) and (d) sample with 6 passes. Image quality map (IQ) - (a) and (c). IQ map overlaid with the spatial distribution of boundaries showing high angle (grains with $\theta > 15^{o}$ - blue lines) and low angle (subgrains with $2 < \theta < 15°$ - red lines) boundaries - (b) and (d)

Figs. 3b and 3d represent the same region of Figs. 3a and 3c, respectively, showing an IQ map overlaid with the spatial distribution of boundaries. After 2^{nd} pass (Fig. 3b), the fraction of high-angle grain boundaries (misorientations $\theta > 15°$ - blue lines) is 68% and

low angle ($2^o < \theta < 15^o$ - red lines) is 32%. After the 6^{th} pass (Fig. 3d), the fraction of high angles was rather similar (61%) although somehow lower. These values indicate partial recrystallization.

Here, it is noteworthy stressing that the low quality of the indexation in the particulate generated "false" high angle grain boundaries. However, for calculating the fraction of high and low angle boundaries, these regions were removed from the maps, and their influence was not considered (please, refer to the supplementary material). The same procedure regarding particulate was used for maps in Figure 4. Better resolution images, regarding grains, can be further observed in the thin foil TEM analysis.

Due to the low magnification, the resolution of the IQ map in Fig. 3a is not as good as expected. Therefore, one could argue whether boundaries around large grains are really grains. Figs. 3e and 3f respectively present a higher magnification IQ map and the IQ map overlaid with the spatial distribution of boundaries, from another region of the sample, free of second particles. Both maps confirm that boundaries in Fig. 3a, and even dense dark-blue zones in Figure 3b, really correspond to grains recrystallizing around old grain boundaries. In fact, these observations confirm the occurrence of the necklace mechanism.

Fig. 4 shows results from strained samples quenched after the interpass time, i.e., it was given some extra time to the material to recover and to recrystallize. Figures 4a-4c represent the sample with 2 passes and interpass time of 5 s. The map of the Inverse Pole Figure (IPF) is shown in Fig. 4a, and the colors are indexed in the IPF displayed in the inset of the figure. It can be observed that there is no preferential orientation after processing. The same fact was observed for all analyzed conditions.

The IQ map presented in Fig. 4b shows that grains are restored after deformation and presents some grains larger than others. The fraction of high-angle boundaries (Fig. 4c) was 81% showing that an almost complete recrystallization took place. Figs. 4d-4f show results from a sample after 6 passes with an interpass time of 20 s. Shapes of grains and the recrystallized volume fraction (81% - Fig. 4e) also indicate an almost full restoration of the material with an average grain size of 25 μm (Fig. 4f).

The IQ map, distribution of boundaries and grain size distribution for a sample with 13 passes and interpass time of 20 s are shown in Figs. 4g to 4i. It can be noticed that some grains are slightly elongated (highlighted with red ellipses, Fig. 4g), suggesting a delay on the recrystallization, which is consistent with the fact that the last passes were conducted at lower temperatures, below the transition temperature. One can infer that these elongated grains represent the lighter regions observed in the optical microscopy (Supplementary Fig. S3). The fraction of high-angle boundaries is around 61% (Fig 4h), which indicates that the recrystallization rate was lower for samples after the transition temperature than for the samples with 2 and 6 passes: this trend was observed in all conditions regardless of the interpass time.

3.3 Analyses of precipitation

The precipitation behaviors for all samples of the VI 58329 were analyzed by carbon extraction replica and thin foils in the TEM. Carbon replica allowed electron diffraction images and microanalysis (EDS) of extracted phases without the interference of the matrix. This technique was also used for counting the number of precipitates, and consequently, to obtain information about the volumetric fraction and the particle density.

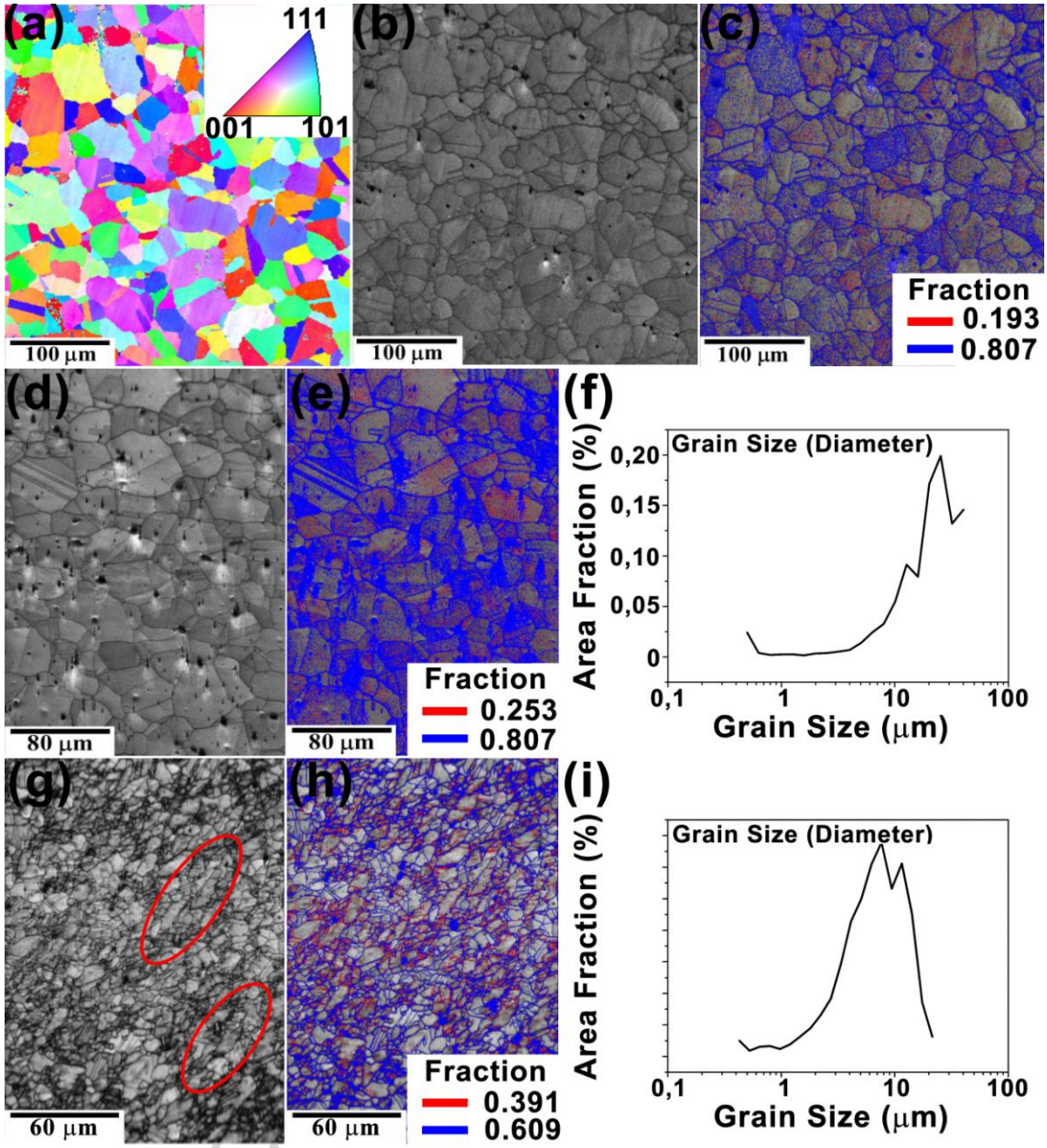

Fig. 4. Images and graphs obtained from EBSD analyses: (a, b, c) after the 2nd pass and interpass time of 5 s; (d, e) and (f) after the 6th pass and interpass time of 20 s; (g, h) and (i) after the 13th pass and interpass time of 20 s. (a) Map of the inverse pole figure (IPF) (color orientation indexation is shown in the IPF presented in the inset). (b, d, g) Image quality (IQ) maps. (c, e, h) IQ map overlaid with the spatial distribution of boundaries showing high angle (grains with $\theta > 15^{o}$ - blue lines) and low angle (–grains with $2 < \theta < 15°$ - red lines) boundaries. (f, i) Distribution of grain sizes

A high-angle annular dark-field (HAADF) detector that present gray tones proportional to the atomic number or to the phase density, also known as Z-contrast, producing images with excellent contrast was used to help distinguishing precipitates from thicker carbon agglomerates produced during the carbon deposition process. With the thin foil technique, was also possible to analyze the interaction between precipitates and grain boundaries or dislocations.

Fig. 5 displays images of Bright Field (BF) Scanning Transmission Electron Microscopy (STEM) from carbon replicas illustrating regions of precipitation in each analyzed condition. Using low magnification, one can observe that the precipitation was not intense up to 6 passes; however, it increased significantly after the transition temperature ($\mathbf{T_T} \approx 13$ passes, Fig. 1). Furthermore, one can infer that, after this latter temperature, the sample with large interpass time (50 s) presented a higher amount of precipitates with larger sizes as compared with those corresponding to interpass times of 20 and 5 s.

Observations with higher magnification showed precipitates with different sizes and shapes (spherical, square-shaped and elongated) for all conditions. As observed for grain sizes, the average size of precipitates decreased with the progress of deformation, and higher quantities of smaller particles appeared with the shortest interpass time.

Details of the quantitative analysis of the precipitates are shown in Fig. 6 and in Supplementary Fig. S4. Fig. 6a shows the average size of the precipitates after counting at least 200 precipitates for each condition. After the soaking time, the mean size of the precipitates was 133 nm; the precipitate size decreased with the applied deformation and shorter interpass times. One exception was for the sample deformed up to 2 passes and 50 s of interpass time, where precipitates had a mean value of 153 nm, indicating that at high temperatures, longer intervals between passes considerably favor the coarsening of

precipitates.

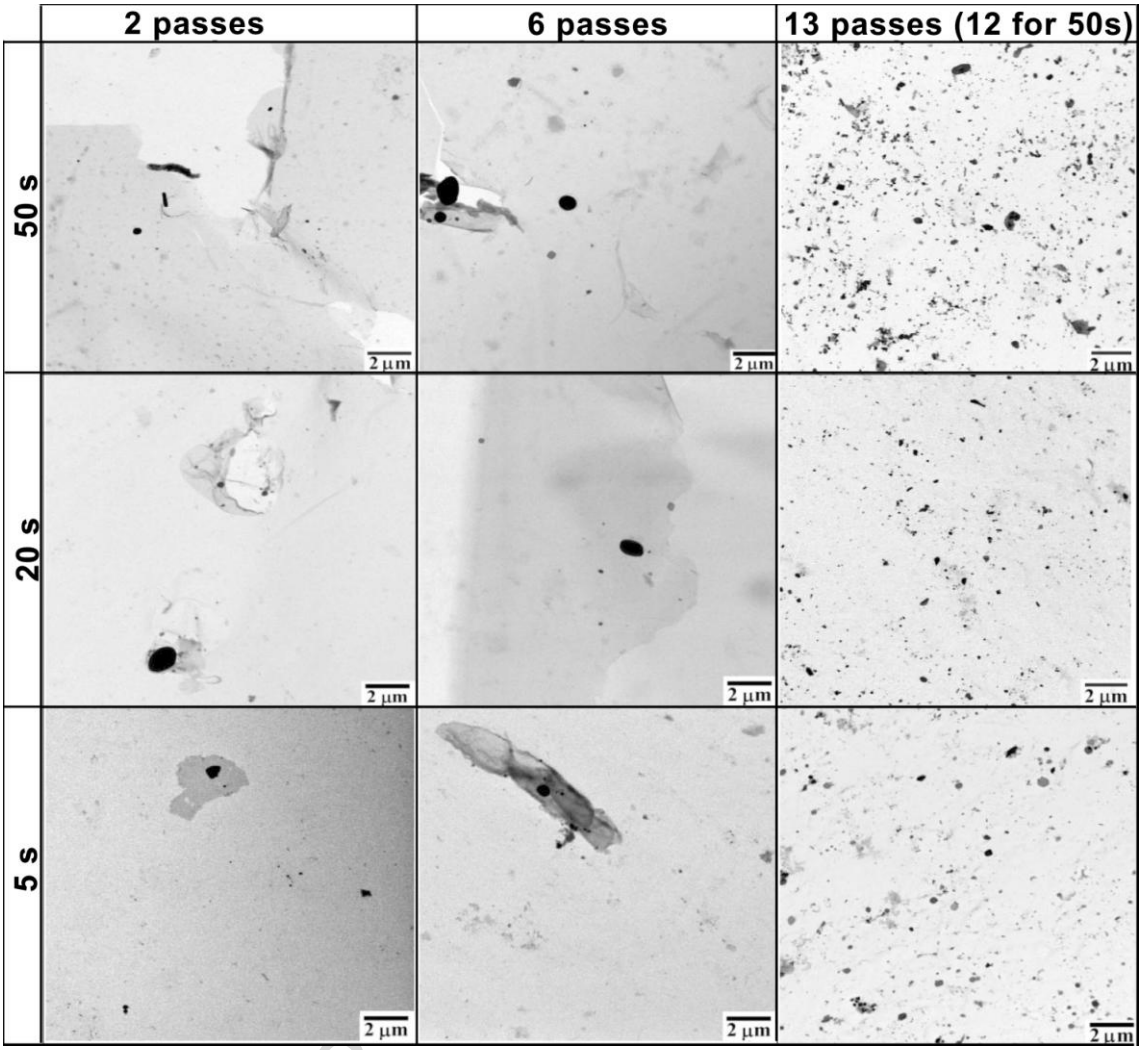

Fig. 5. Bright Field Images from Scanning Transmission Electron Microscopy (STEM) micrographs of carbon replica after 2nd, 6th e 13th (12th for 50 s) passes with interpass times of 50, 20 e 5s

Figure 6b displays the distribution of precipitate sizes in terms of relative frequency for all conditions tested. It can be seen that after two passes, most of the precipitates were greater than 100 nm, and the amount of larger precipitates increased with the increasing of interpass time. After the 6th pass and interpass times of 20 and 5 s there were considerable amounts of precipitates smaller than 50 nm, and a higher

quantity with sizes above 50 nm. Distribution profiles at low temperatures (13 passes) show that most of the precipitates have had sizes below 50 nm, regardless the interpass time. With an interpass time of 5 s, the amount of these small particles was higher.

Supplementary Figures S4a and S4b show the particle density (part /μm2) and volume fraction of precipitates, respectively. One can observe that at high temperatures (2^{nd} and 6^{th} passes), the density of particles was low and increased considerably after the transition temperature ($\mathbf{T_T}$). Moreover, the volume fraction shows variable behavior, where higher interpass times and high temperatures helped the growing of precipitates.

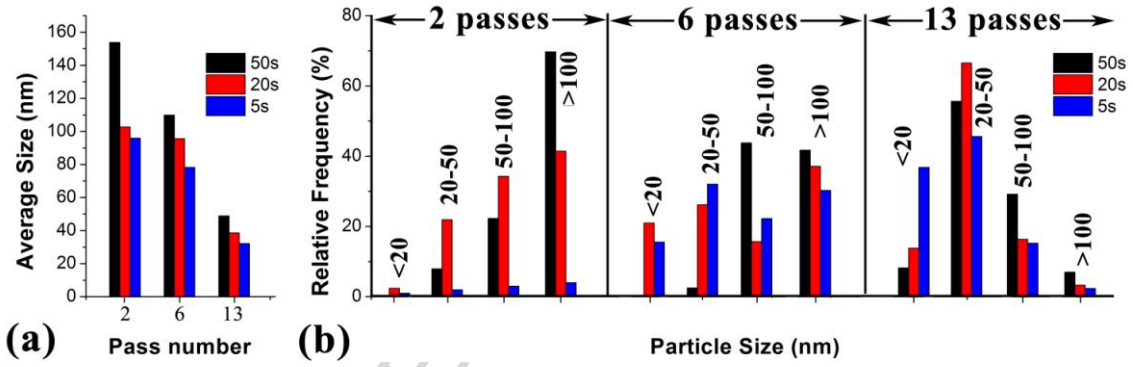

Fig. 6. (a) Average precipitate sizes as a function of the number of passes. (b) Distribution of particle sizes: 2^{th} pass, 6^{th} pass and 13^{th} pass

The analysis and chemical composition of precipitates observed in the sample with 12 passes and interpass time of 50 s are shown in the Supplementary Fig. S5. It is readily apparent that below the transition temperature, precipitation was more intense than above it. Moreover, one can observe that the precipitates had different morphologies (square-shaped, rounded and elongated) and several sizes. In this figure only the precipitate number 1, larger than 200 nm, exhibited titanium in significant proportion; thus, this precipitate can be considered as an undissolved particle coming

from the soaking process. Other precipitates did not present significant differences in their compositions, except precipitate 12 that showed a higher content of niobium. Quantitative analysis of all samples showed that only 4.8% of particles were NbN. The rest was the Z-phase, regardless the shape and size of the precipitates. Selected area electron diffraction patterns (SADP) helped to identify the precipitates as shown in the Supplementary Figure S5c, indexed as TiNbN, and in Figure S5d, indexed as CrNbN (Z-phase).

Investigations of the interaction between precipitates with grain boundaries and dislocations were carried out using thin foils. Fig. 7 illustrates micrographs in some conditions, although samples have been analyzed in all testing conditions with this technique. Fig. 7a shows small and large precipitates in a microstructure with small grain size from one region of the steel in the as-received condition. After soaking, where the grains grew considerably, it was observed that most of the particles were dissolved. The ones that remained insoluble were large and mostly with elongated morphology, as shown in Fig. 7b. A representative image of the sample with 6 passes and interpass time of 5 s is shown in Fig. 7c. Note the presence of large particles (> 100 nm), some of them located at grain boundaries. Inspection of other regions within the sample confirmed that there was no intense precipitation under this condition. In an additional experiment conducted in a sample that was cooled to 1000^{o}C after soaking without application of deformation, it was observed (see Fig. 7d) that precipitates nucleated preferably inside the grains, and they were small. It is worth noting that this sample was water quenched below the transition temperature.

The last pictures are related to samples after the transition temperature with interpass times of 50 s (Fig. 7e) and 20 s (Fig. 7f) under conditions where an intense

precipitation was noticed. Fig. 7e also shows the interface between a recrystallized and a non-recrystallized region, as can be inferred by the free-of-dislocations region on the left-hand side, and the forest of dislocations on the right-hand side. In both regions, precipitates are easily observed. Furthermore, it should be highlighted the interaction between precipitates and dislocations how they are pinning grain boundaries, especially in the lower right-side of the image. On the contrary, Fig. 7f displays a region with plenty of precipitates, with an average size of 50 nm, interacting with the substructure. Arrows indicate some of these interactions: red arrows show precipitates along dislocations; the green arrow indicates interaction with subgrain boundaries and the blue arrow with a high-angle grain boundary.

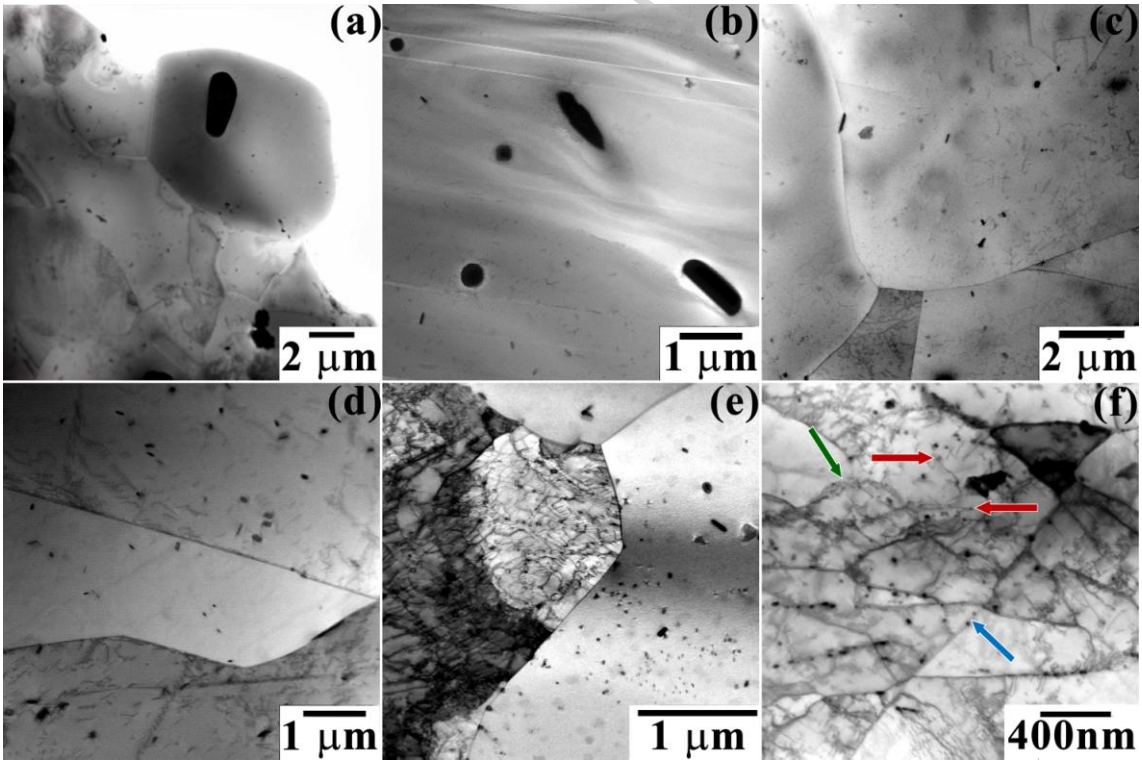

Fig. 7. Thin foils TEM analysis in the following conditions: (a) as-received; (b) T_{soak} = 1250^{o}C (5 min); (c) with t_{ip} = 5 s after the 6th pass; (d) on cooling at 1000°C without deformation; (e) after 12th pass and t_{ip} = 50 s; (f) after 13th pass with t_{ip} = 20 s

4 - DISCUSSION

The reheating temperature and the pass schedule during the metallurgical processing of steels under continuous cooling conditions are important because they determine their final microstructure and, consequently, their mechanical properties. The parameters that control the thermomechanical processing can be changed and new processing routes can be used to improve the microstructures and therefore, the final mechanical properties. The steel investigated in this study presented an average grain size of 62 μm when soaked at 1250°C for 5 min; this grain size may be considered small when compared to grain sizes obtained for niobium-microalloyed steels and austenitic stainless steels without precipitates under the same soaking conditions [25-28]. The precipitation analysis showed that only TiNbN particles with large sizes remained insoluble after soaking. However, most of the niobium was dissolved and was in solid solution indicating that this element was ready to precipitate during cooling. It is well established that niobium in solid solution delays the grain growth during austenitization and enhances the Z-phase precipitation upon metallurgical processing.

At the beginning of pass schedules, the average density of precipitates changed very little, as shown in Supplementary Figure S4a. This fact may be due to the supersaturation necessary for nucleation of new precipitates. On the other hand, one can observe in Fig. 1 and Supplementary Fig. S1 that the stress in the 1st pass is greater than in the 2nd pass, which in turns is larger than in the 3rd pass, mainly for longer interpass times. This is not the usual behavior of metallic materials, whose strength increases with decreasing temperature. Since precipitates act as obstacles to dislocation motion, one can expect that precipitates present in the 1st pass increase the strength of the material. One can speculate that during deformation some undissolved particles were fragmented

or dissolution could take place inasmuch as the soaking time was relatively small (300 s) and equilibrium condition could not be reached. During subsequent interpass times, precipitates grew, as indicated in Fig. 6a and Supplementary Fig. S4b. Precipitate coarsening, combined with phenomena of static softening, decreased the material's strength more than the expected increment caused by temperature diminution. It is worth noticing that the decrease in stress level was more significant for longer interpass times.

Along with the decreasing of stress level in the 2nd and 3rd passes, one can also observe in Figures 1 and S1 that the stress necessary at the onset of deformation in the second pass is lower than that observed at the end of the first pass. The same is true for the second and third passes independently of the interpass times. This is a clear indication that some amount of static recrystallization took place between these passes. Figures 4 and 5 show a partially recrystallized microstructure immediately after the second pass and full recrystallization after the interpass time, before the third pass. Additionally, it can be associated with the fact that larger particles are not effective in delaying recrystallization. A similar aspect appears in Figures 2 and 3, where it is noticed partial recrystallization after the 6th pass and full recrystallization after the interpass time.

Although recrystallization was observed in all passes, some difference can be seen after the 13th pass: only partial recrystallization occurred. The evolution of the MSF in Figure 1 indicates that, after the 3rd pass, the stress continuously increased with the inverse of the absolute temperature. However, this increasing is more considerable after the pass number 7 or 8. Looking at Fig. 5 clearly precipitation significantly increased at lower temperatures. Fig. 6b displays that, after 13 passes, most of the

particles were smaller than 50 nm, and the density (Supplementary Fig. S4a) and volume fraction (Supplementary Fig. S4b) significantly increased (it should be borne in mind that the average size was 130 nm after soaking). Upon straining the stored energy is increased due to the rise of crystalline defects. Regions with higher free energy such as dislocations and subgrain boundaries become sites for nucleation of new particles such as the Z phase. Strain-induced precipitations immobilize the substructure inhibiting the recrystallization as already shown in Figures 7e and 7f where precipitates interact with dislocations, subgrains and grain boundaries.

Another important aspect of the interaction between precipitates and grain boundaries is how precipitates can inhibit grain growth after recrystallization. Particle density, which increases sharply at lower temperatures (Supplementary Fig. S4a), and volume fraction (Supplementary Fig. S4b) were used in calculations to stipulate the expected average critical radius to promote pinning of grain boundaries. The critical radius calculated using the equations proposed by Zener, Gladman, Hillert and Rios [29] together with the average radii measured in the samples are presented in Table 1.

In these equations, r corresponds to the average radius of precipitates and f their volume fraction. In the Gladman's equation, Θ is the ratio of the maximum radius of the grains and their average radius, and represents the heterogeneity of grain size distribution in the sample. In general, critical radiuses found by Zener equation are larger than those obtained in this work. On the contrary, the equation proposed by Rios predicted smaller grain sizes than the actual ones. The estimated values using equations of Gladman and Hillert were the closest to the measured radii. Accordingly, after most deformation passes, the presence of particles (most of them stimulated by deformation) would be hindering recrystallization and grain growth, but the particle coarsening

between passes would be decreasing the critical radius, and therefore allowing recrystallization and grain growth to take place. This recrystallization will not be complete due to lack of interpass time and presence of solute atoms that delay the recrystallization kinetics.

Table 1. Grain size evolution as a function of pass number and compared with Critical radius (Rc) calculated using the Zener, Gladman, Hillert and Rios formulas [29]

		$R_{experimental}$ (μm)	$R_{critical}$ (μm)			
			Zener 4r/3f	**Gladman r/f[π(0.25-0.33/θ)]**	**Hillert 0.44r/f**	**Rios 0.17r/f**
1250°C/5 min		30.92	91.64	31.90	30.24	11.68
2 passes	**50 s**	16.66	25.60	11.48	8.45	3.26
	20 s	16.32	48.46	20.31	15.99	6.18
	5 s	15.33	34.21	7.66	11.29	4.36
6 passes	**50 s**	16.99	24.49	7.94	8.08	3.12
	20 s	12.09	72.35	28.36	23.88	9.22
	5 s	7.50	38.20	13.00	12.60	4.87
12 or 13 passes	**50 s**	5.53	3.83	1.59	1.26	0.49
	20 s	4.74	5.65	2.28	1.86	0.72
	5 s	2.57	7.71	2.73	2.54	0.98

5 - SUMMARY AND CONCLUSIONS

The simulation of thermomechanical processing by hot torsion testing allowed following the microstructure evolution and mechanical behavior of the austenitic stainless steel during pass schedules on continuous cooling conditions. After characterization, the following conclusions can be drawn:

- ✓ After the soaking time, only undissolved TiNbN particles were found. These larger particles did not retard the recrystallization but increased the hot strength of the material.
- ✓ Coarsening of precipitates during interpass times decreased the strength of the material.
- ✓ Niobium in solid solution delays the grain growth upon soaking time and nucleates the Z-phase and NbN precipitates upon metallurgical processing.
- ✓ Dynamic recrystallization acted in all passes, providing an excellent grain refinement. Recrystallization was complete at high temperatures and partial below the transition temperature ($\mathbf{T_T}$). At lower temperatures, strain-induced precipitations took place and immobilized the substructure retarding the recrystallization and increasing the flow stress level.
- ✓ The grain refinement was greater below the transition temperature; smaller grain sizes were obtained with shorter interpass time, although the final microstructure was not homogeneous because it consisted of recrystallized and non-recrystallized grains.

Acknowledgements

The authors are grateful to CNPq (Conselho Nacional de Desenvolvimento Científico e Tecnológico), FAPESP (Fundação de Amparo à Pesquisa do Estado de São Paulo) and CAPES (Coordenação de Aperfeiçoamento de Pessoal de Nível Superior) for the financial support received in the development of this project and Villares Metals, São Paulo-Brazil, that supplied the steel. Also authors are grateful to CAPES (Brazil) and Ministerio de Educacion (Spain) for funding a bilateral cooperation, under the

cooperation project CAPES#179/09.

References

[1] Y. Murata, S. Ohashi, Y. Uematsu, Recent trends in the production and use of high strength stainless steels. ISIJ Intern. 33 (1993) 711-720. DOI: 10.2355/isijinternational.33.711

[2] P. Shankar, H. Shaikh, S. Sivakumar, S. Venugopal, D. Sundararaman, H.S. Khatak, Effect of thermal aging on the room temperature tensile properties of AISI type 316LN stainless steel. J. of Nucl. Mater. 264 (1999) 29-34.

[3] K.H. Lo, C.H. Shek, J.K.L. Lai, Recent developments in stainless steels. Mater. Sci. Eng. R, 65 (2009) 39-104. DOI: 10.1016/j.mser.2009.03.001

[4] E.J. Giordani, A.M. Jorge Jr, O. Balancin, Evidence of strain-induced precipitation on a Nb- and N-bearing austenitic stainless steel biomaterial. Mater. Sci. Forum. 500-501 (2005) 179-186. DOI: 10.4028/www.scientific.net/MSF.500-501.179

[5] E.S. Silva, R.C. Souza, A.M. Jorge Jr, O. Balancin, Hot deformation behavior of an Nb- and N-bearing austenitic stainless steel biomaterial. Mater. Sci. Eng. A, 543 (2012) 69-75. DOI: 10.1016/j.msea.2012.02.048

[6] R.C. Souza, E.S. Silva, A.M. Jorge Jr, J.M. Cabrera, O. Balancin, Dynamic recovery and dynamic recrystallization competition on a Nb- and N-bearing austenitic stainless steel biomaterial: Influence of strain rate and temperature. Mater. Sci. Eng. A, 82 (2013) 96-107. DOI: 10.1016/j.msea.2013.06.037

[7] M.B.R. Silva, J. Gallego, J.M. Cabrera, O. Balancin, A.M. Jorge Jr, Interaction

between recrystallization and strain-induced precipitation in a high Nb- and N-bearing austenitic stainless steel: Influence of the interpass time, Mater. Sci. Eng. A. 637 (2015) 189-200. DOI: 10.1016/j.msea.2015.04.049

[8] P.W. Robinson, D.H. Jack, Precipitation of Z -phase in a high-nitrogen stainless steel. J. Heat Treat. 4 (1985) 69-74. DOI: 10.1007/BF02835491

[9] H.K. Danielsen, J. Hald, F.B. Grumsen, M.A. Somers, On the crystal structures of Z-phase Cr(V,Nb)N. Metall. Mater. Trans. A, 37 (2006) 2633-2640. DOI: 10.1007/BF02586098

[10] A. Golpayegani, H. Andrén, H. Danielsen, J. Hald, A study on Z-phase nucleation in martensitic chromium steels. Mater. Sci. Eng. A, 489 (2008) 310-318. DOI: 10.1016/j.msea.2007.12.022

[11] E.J. Giordani, V.A. Guimarães, T.B. Pinto, I. Ferreira, Effect of precipitates on the corrosion-fatigue crack initiation of ISO 5832-9 stainless biomaterial. Int. J. Fatigue. 26 (2004) 1129-1136. DOI: 10.1016/j.ijfatigue.2004.03.002

[12] C. Örnhagen, J-O Nilsson, H. Vannevik, Characterization of a nitrogen-rich austenitic stainless steel used for osteosynthesis devices. J. Biomed. Mater. Res. 31 (1996) 97-103. DOI: 10.1002/(SICI)1097-4636(199605)31:1<97::AID-JBM12>3.0.CO;2-J

[13] H.K. Danielsen, J. Hald, On the nucleation and dissolution process of *Z*-phase Cr(V,Nb)N in martensitic 12%Cr steels. Mater. Sci. Eng. A. 505 (2009) 169-177. DOI: 10.1016/j.msea.2008.11.019

[14] L. Cipolla, H.K. Danielsen, D. Venditti, P.E. Di Nunzio, J. Hald, M.A.J. Somers, Conversion of MX nitrides to *Z*-phase in a martensitic 12% Cr steel. Acta Mater. 58 (2010) 669-679. DOI: 10.1016/j.actamat.2009.09.045

[15] R.O. Kaibyshev, V.N. Skorobogatykh, A. Shchenkova, Formation of the *Z*-phase and prospects of martensitic steels with 11% Cr for operation above 590^{o}C. Metal Sci. Heat Treat. 52 (2010) 90-99. DOI: 10.1007/s11041-010-9239-0

[16] J. Erneman, M. Schwind, P. Liu, J.-O. Nilsson, H.-O. Andrén, J. Agren, Precipitation reactions caused by nitrogen uptake during service at high temperatures of niobium stabilised austenitic stainless steel. Acta Mater. 52 (2004) 4337-4350. DOI: 10.1016/j.actamat.2004.06.001

[17] L. Cipolla, H.K. Danielsen, P.E. Di Nunzio, D. Venditti, J. Hald, M.A.J. Somers, On the role of Nb in *Z*-phase formation in a 12% Cr steel. Scr. Mater. 63 (2010) 324-327. DOI: 10.1016/j.scriptamat.2010.04.025

[18] V. Vodárek, Creep behaviour and microstructural evolution in AISI 316LN + Nb steels at 650^{o}C. Mater. Sci. Eng. A. 528 (2011) 4232-4238. DOI: 10.1016/j.msea.2011.02.025

[19] C. Kocer, T. Abe, A. Soon, The *Z*-phase in 9-12% Cr ferritic steels: A phase stability analysis. Mater. Sci. Eng. A. 505 (2006) 1-5. DOI: 10.1016/j.msea.2008.10.028

[20] T. Sourmail, Precipitation in creep resistant austenitic stainless steels. Mater. Sci. Technol., 17 (2001) 1-14. DOI: 10.1179/026708301101508972

[21] H.K. Danielsen, J. Hald, F.B. Grumsen, M.A.J. Somers, On the crystal structures of *Z*-phase Cr(V,Nb)N. Metall. Mater. Trans. A. 37 (2006) 2633-2640. DOI: 10.1007/BF02586098

[22] A.J. Deardo, Niobium in modern steels. Int. Mater. Rev. 48 (2003) 371-402. DOI: DOI: 10.1179/095066003225008833

[23] S. Vervynckt, K. Verbeken, B. Lopez, J.J. Jonas, Modern HSLA steels and role of

non-recrystallization temperature. Int. Mater. Rev. 57 (2012) 187-207. DOI: 10.1179/1743280411Y.0000000013

[24] R.J. Seher, H.M. James, G.N. Maniar, Quantitative metallography of the age hardening precipitation in superalloys by replica electron microscopy. Symposium: Am. Soc. Test. Mater. (1971) 119-137.

[25] F. Boratto, R. Barbosa, S. Yue, J.J. Jonas, Effect of chemical composition on the critical temperatures of microalloyed steels. Int. Conf. Phys. Metall. Thermomec. Process. Steels and Other Metals (Thermec-88), ISIJ, Tokyo, Japan, 1988, pp.383-390.

[26] S. Vervynckt, K. Verbeken, P. Thibaux, M. Liebeherr, M.; Houbaert, Y. Austenite recrystallization-precipitation interaction in niobium microalloyed steels. ISIJ Int. 49 (2009) 911-920. DOI: 10.2355/isijinternational.49.911

[27] S. Vervynckt, K. Verbeken, P. Thibaux, Y. Houbaert, Recrystallization-precipitation interaction during austenitic hot deformation of Nb microalloyed steel. Mater. Sci. Eng. A, 528 (2011) 5519-5528. DOI: 10.1016/j.msea.2011.03.087

[28] B. Dutta, E. Valdes, C.M. Sellars, Mechanism and kinetics of strain induced precipitation of Nb(C,N) in austenite. Acta Metall. Mater. 40 (1992) 653-662. DOI: 10.1016/0956-7151(92)90006-Z

[29] P.A. Manohar, M. Ferry, T. Chandra, Five decades of the Zener equation. ISIJ Int. 38 (1998) 913-924. DOI: 10.2355/isijinternational.38.913

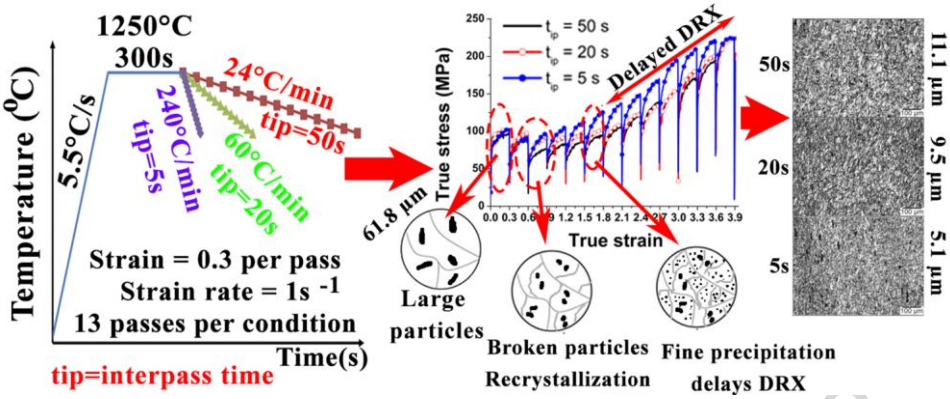

Graphical abstract

Highlights

Thermomechanical controlled processing was applied to ISO 5832-9 steel

TiNbN was undissolved after soaking, Z-phase and NbN precipitated during processing.

ISO 5832-9 steel behaves alike to microalloyed steel,

Dynamic recrystallization is delayed after a characteristic temperature

The shorter the interpass time, the higher the grain refinement.